Journal of Experimental Psychology:
Human Perception and Performance
1999, Vol. 25, No. 2, 426–444

0096-1523/99/$3.00

Perceiving Surface Slant From Deformation of Optic Flow

Fulvio Domini and Corrado Caudek
Cognitive Technology Laboratory, AREA Science Park

Perceived surface orientation and angular velocity were investigated for orthographic projections of 3-D rotating random-dot planes. It was found that (a) tilt was accurately perceived and (b) slant and angular velocity were systematically misperceived. It was hypothesized that these misperceptions are the product of a heuristic analysis based on the deformation, one of the differential invariants of the first-order optic flow. According to this heuristic, surface attitude and angular velocity are recovered by determining the magnitudes of these parameters that most likely produce the deformation of the velocity field, under the assumption that all slant and angular velocity magnitudes have the same a priori probability. The results of the present investigation support this hypothesis. Residual orientation anisotropies not accounted for by the proposed heuristic were also found.

The relative motion between the eye and the environment gives rise to a changing retinal projection that encodes useful information about the layout of the environment and the motion of the observer. Several mathematical analyses have shown that perspective projections of points lying at different depths from the observer encode useful information about the layout of the environment (Koenderink, 1986; Koenderink & Van Doorn, 1975, 1976; Longuet-Higgins & Prazdny, 1980; Prazdny, 1980). Moreover, other mathematical analyses have shown that, under the assumptions of rigidity (Bennett, Hoffman, Nicola, & Prakash, 1989; Hoffman, 1982; Ullman, 1979) or fixed-axis motion (Hoffman & Bennett, 1985, 1986), the recovery of 3-D structure is theoretically possible also from parallel projections of rotating objects.

The present article focuses on the limiting case of a dynamic projection characterized by a *linear velocity field.* A linear velocity field can be produced, for example, by the translation of an observer relative to a planar surface or by the rotation of a local planar patch induced by the motion of an observer fixating a point of a stationary object.

To explain our motivation for conducting the experiments reported here, we first discuss some relevant properties of the linear velocity field. We then introduce some notions necessary to define the orientation of a surface in 3-D space, and finally, we relate the properties of the first-order optic flow to the orientation of a surface.

A *velocity field* is defined as a function associating a velocity vector with each point (u, v) of the projection plane.[1] The linear velocity field represents a simple case of a velocity field. Koenderink and Van Doorn (1990) have shown that, after the image plane rotation and the expansion or contraction components are subtracted, a linear velocity field reduces to a field of parallel velocity vectors. Such a velocity field can be described by the following linear equations:

$$V_u = \phi_u u + \phi_v v + V_{ut}$$

$$V_v = 0, \tag{1}$$

where u, v are the 2-D image plane coordinates, ϕ_u and ϕ_v are the horizontal and vertical gradients, and V_{ut} (the common translatory component) represents the velocity at the origin of the coordinate system (i.e., the average velocity in a local neighborhood of the velocity field). Figure 1 shows three examples of a linear velocity field.

An important property of a velocity field is the deformation (*def*), the square root of the sum of the squared horizontal and vertical gradients (see Figure 1):

$$def = \sqrt{\phi_u^2 + \phi_v^2}. \tag{2}$$

Def is important because, as shown in the following sections, it is informative about the motion and orientation parameters of a projected *planar surface* (see also Koenderink, 1986). The experiments described in the present article were designed to examine the relationship between perceived orientation of a 3-D planar patch and *def.*

Fulvio Domini and Corrado Caudek, Cognitive Technology Laboratory (a collaboration between the Department of Psychology of the University of Trieste and INSIEL SpA, a software company), AREA Science Park, Trieste, Italy.

Correspondence concerning this article should be addressed to Fulvio Domini, who is now at the School of Optometry, 506 Minor Hall, University of California, Berkeley, California 94720. Electronic mail may be sent to fulvio@john.berkeley.edu.

[1] In the present article, the velocity field is considered to be the input to the perceptual system that derives 3-D structure from projected motion. It is important to point out, however, that an exact encoding of the velocity field requires knowledge of the absolute distance from the eye to the image plane. Because absolute distance information can be estimated only by the perceptual system, the encoded properties of the velocity field will also be accordingly approximated. In the following discussion, therefore, what we call "*distance* to the image plane" should be understood as "*perceived distance* to the image plane."

$$\phi_u = \frac{V_u(\Delta u, 0) - V_u(0,0)}{\Delta u} \qquad \phi_v = \frac{V_u(0, \Delta v) - V_u(0,0)}{\Delta v}$$

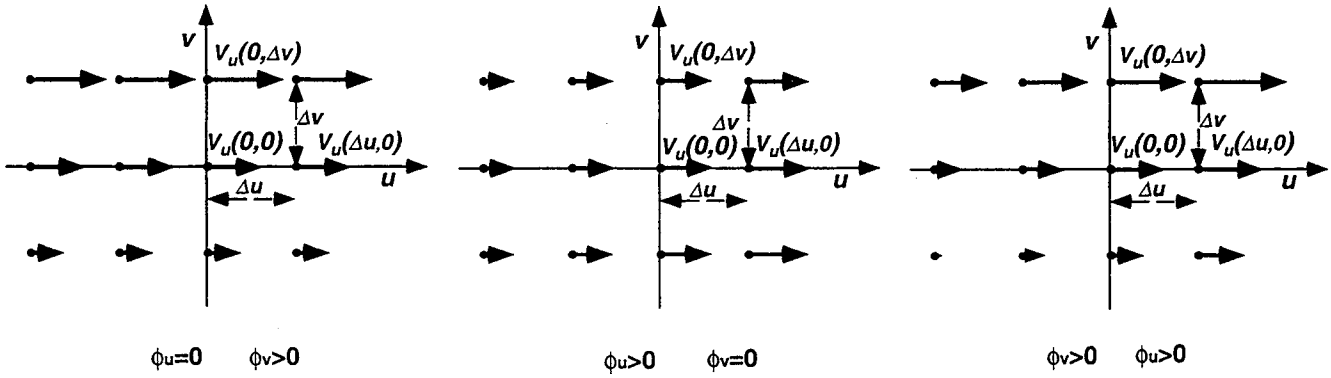

Figure 1. Schematic representation of a linear velocity field in which u and v represent the horizontal and vertical dimensions, respectively. Each arrow represents an instantaneous velocity vector V. Left panel: The velocity gradient in the v direction is nonzero and ϕ_u is nil. Middle panel: The velocity gradient in the u direction is nonzero and ϕ_v is nil. Right panel: Both ϕ_u and ϕ_v are different from zero.

A planar surface in 3-D space can be described as

$$z = g_1 x + g_2 y, \tag{3}$$

where g_1 and g_2 are the two components of the depth gradient (see Figure 2). The 3-D orientation of a surface, however, is usually described in terms of slant and tilt, rather than in terms of g_1 and g_2. The slant is (the tangent of) the angle between the surface and the image plane, and it is defined as $\sigma = \sqrt{g_1^2 + g_2^2}$. The tilt is the angle of rotation of the surface in the image plane, and it is defined as $\tau = \arctan(g_2/g_1)$. An exemplification of these notions is presented in Figures 3 and 4.

The local velocity field produced by a surface undergoing a generic motion under a perspective projection can be approximated by a linear velocity field (Hoffman, 1982). If the motion of the surface is planar (i.e., if the surface rotates

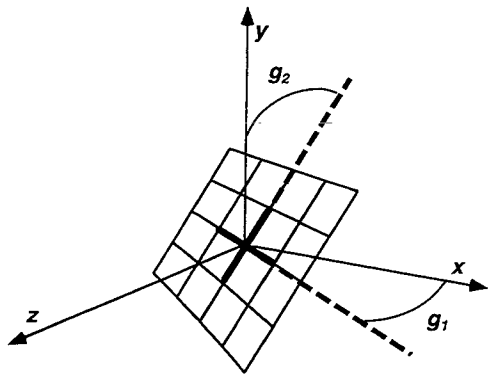

Figure 2. Schematic representation of a planar surface with its center coinciding with the center of the (x, y, z) coordinate system and in which g_1 and g_2 are the horizontal and vertical components of the depth gradient, respectively. The amount of (the tangent of) rotation of the surface about the y-axis is represented by g_1, and g_2 represents the amount of (the tangent of) rotation about the x-axis.

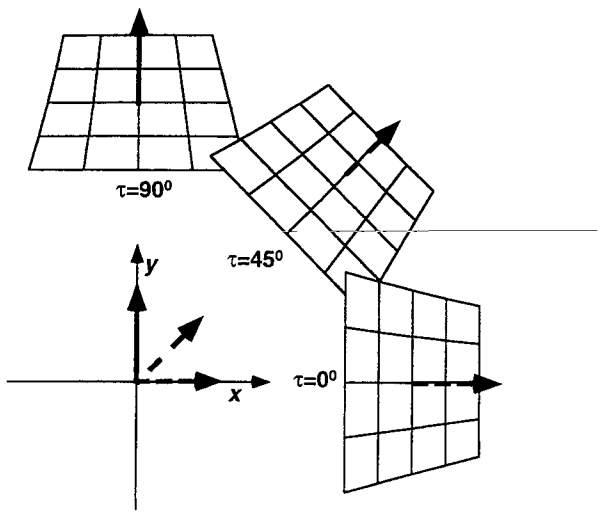

Figure 3. Schematic representation of a planar surface with a slant of tan (45°) and three different tilt (τ) magnitudes: τ = tan (90°), τ = tan (45°), and τ = tan (0°). The arrows in bold represent the normal to the plane. Tilt is defined as the tangent of the angle between the projection of the normal to the surface and the x-axis.

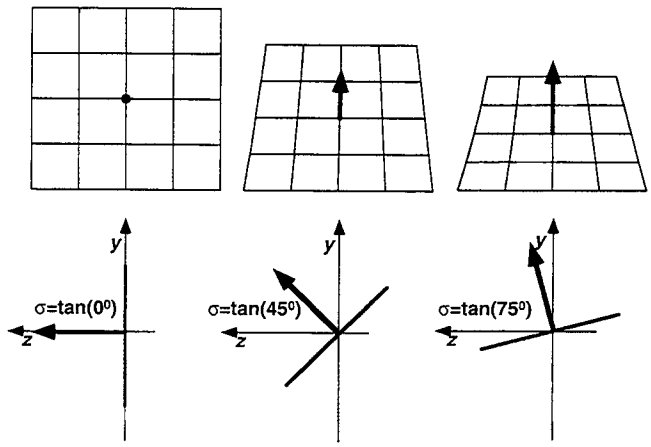

Figure 4. Schematic representation of a planar surface with a tilt of 90° and three different slant (σ) magnitudes: σ = tan (0°), σ = tan (45°), and σ = tan (75°). The arrows in bold represent the normal to the surface (in the case of σ = 0, τ is not defined). Slant is defined as the tangent of the angle between the normal to the surface and the z-axis.

about the y-axis and translates parallel to the x–z plane), then, as shown in Appendix A, the local velocity field can be approximated by

$$V_u \approx (g_1 u + g_2 v)\left(\omega + \frac{V_x}{e}\right) + V_x, \tag{4}$$

where u, v are the coordinates of the projected points; g_1 and g_2 are the horizontal and vertical gradients, respectively, of a local planar patch; V_x is the translatory velocity in the x direction; ω is the rotatory velocity about the y-axis; and e is the distance of the vantage point from the image plane (see Figure 5). Appendix A shows that the deformation and the translatory component of this velocity field are

$$def = \sigma\left(\omega + \frac{V_x}{e}\right)$$

$$V_{ut} = V_x. \tag{5}$$

The information provided by *def*, V_{ut}, and the eye distance (e) is not sufficient to uniquely determine the distal parameters σ and ω because the previous system of equations is underconstrained. This means, therefore, that under a perspective projection, the linear velocity field is ambiguous.

If it is assumed that the rotatory component of the 3-D motion is nil (ω = 0), then Equation 4 reduces to the equation of a motion parallax velocity field. In this particular case, *def* and V_{ut} uniquely determine the distal parameters σ and V_x. The ratio def/V_{ut}, in fact, is proportional to the simulated slant:

$$\frac{def}{V_{ut}} = \frac{\sigma}{e}. \tag{6}$$

For a *motion-parallax* velocity field, therefore, the first-order optic flow is in principle informative about projected slant. The relevance of this information for human observers has been demonstrated by many psychophysical investigations (Braunstein, 1962, 1966, 1968; Braunstein & Andersen, 1981; Braunstein, Liter, & Tittle, 1993; Braunstein & Tittle, 1988; Clocksin, 1980; Graham & Rogers, 1982; Loomis & Eby, 1988; Ono, Rivest, & Ono, 1986; Rogers & Collett, 1989; Rogers & Graham, 1979, 1982, 1983).

The purpose of the present article is to study the perceptual interpretation of a particular case of the linear velocity field, that is, the velocity field characterized by a nonzero *def* component and a nil V_{ut} component. Such a velocity field does not uniquely specify the orientation and motion parameters of a projected surface. Such a particular case arises, for example, when an observer moving in the environment fixates a point on a surface. The point toward which the observer directs his or her gaze projects as a stationary feature on his or her retina, and the surrounding velocity field is characterized by a pure *def* (see Figure 6).

When the translatory component V_{ut} is equal to zero, the deformation component reduces to

$$def = \sigma\omega. \tag{7}$$

Equation 7 shows, therefore, that a pure *def* velocity field is ambiguous because infinite pairs of slants and angular velocities produce the same magnitude of deformation.

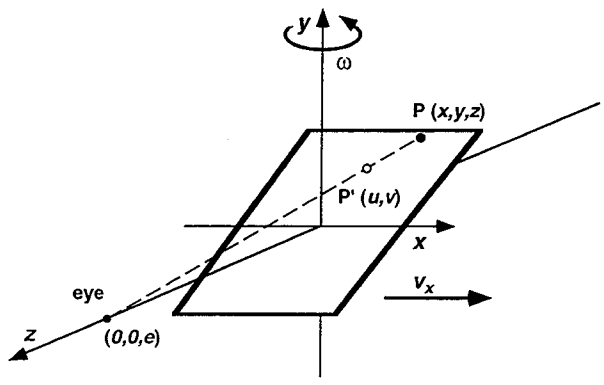

Figure 5. Schematic representation of a planar surface rotating about the y-axis (with angular velocity ω) and translating in a direction parallel to the x–y plane (with translatory velocity V_x). The distance between the center of projection and the x–y plane is e. P is a generic point on the surface, and P' is the projection of P on the x–y plane.

Relation Between *def* and Surface Motion and Orientation

Because the present investigation focuses on the influence of *def* on perceived surface attitude, it is worthwhile to present some examples providing an intuitive understanding of this property of the velocity field. Figure 7 shows the

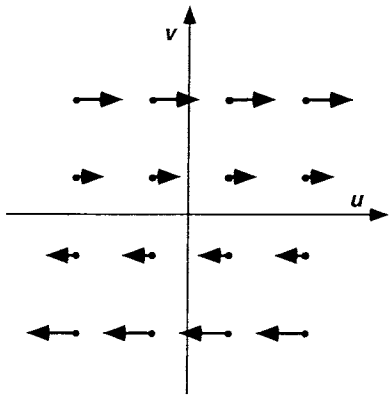

Figure 6. Schematic representation of a pure *def* velocity field produced by the rotation of a planar patch about the *y*-axis. Notice that the translatory component (i.e., the mean of the [signed] instantaneous velocities) is equal to zero.

projective transformations produced by the orthographic projection of a planar surface undergoing a 3-D rotation about an axis parallel to the surface (the *y*-axis in Figure 7). In this particular case, *def* is proportional to the magnitude of horizontal compression in the image plane projection of the checkerboard. Figure 7, however, illustrates only a particular case of the projective transformations that define *def*. For a generic initial orientation of the checkerboard, in fact, a rotation about the vertical axis produces a change in both the *x* and *y* components of the depth gradient. As shown in Figure 8, the projective transformations of a checkerboard with a generic orientation exhibit both a compression in the *x*-dimension and a transversal "stretching" (middle bottom panel). Because in the generic case both of these components are present, the magnitude of *def* is difficult to visualize. For this reason, we are restricting the present discussion to the particular case shown in Figure 7.

Equation 7 indicates that infinite pairs of angular velocities and slants produce the same magnitude of *def*. This ambiguity is illustrated in Figure 9. In the left panel, five checkerboards are depicted as in Figures 7 and 8. The middle panel shows that each checkerboard has a different initial orientation and undergoes a different amount of rotation. The initial orientation of the checkerboards and the magnitudes of their rotation were chosen so as to produce the same amount of horizontal compression in the (*x*–*y*) image plane. This illustrates, therefore, that the same 2-D transformations can be produced by coupling different initial slants with different magnitudes of rotation. A subset of the infinite possible combinations of slant and angular rotation magnitudes compatible with the 2-D transformations used in this example is shown in the right panel of Figure 9. In this plot, the *x*-axis represents the magnitude of angular rotation (ω), and the *y*-axis represents the magnitude of initial slant (σ) of the checkerboard. The dots represent the five combinations of σ and ω illustrated in the left panel.

Deformation and Perceived Structure From Motion

Equation 6 shows that within a geometrically correct analysis of the optic flow, *def* and V_{ut} are informative about

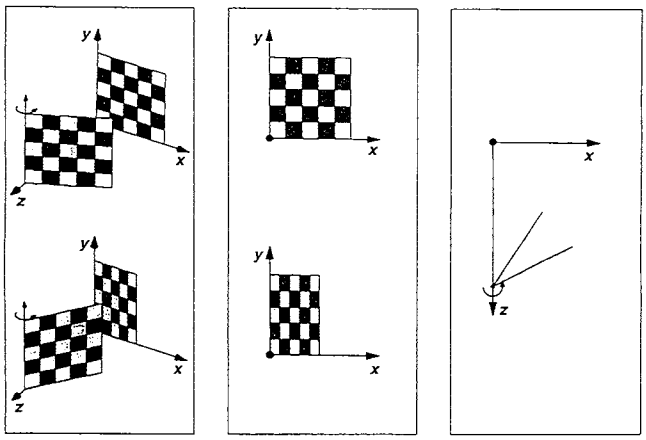

Figure 7. Left panel: A checkerboard within a coordinate system in which the *x* and *y* axes represent the image plane and the *z*-axis represents the line of sight. The checkerboard plane is parallel to the *y*-axis. The checkerboard is represented before (top) and after (bottom) 30° of rotation about an axis parallel to the *y*-axis. The checkerboard has been predeformed so that, before rotation, each surface element projects on the image plane as a square (on the checkerboard the surface elements are not shaped as squares). The figure depicts both the checkerboard (front) and its orthogonal projection on the (*x*–*y*) image plane (back). Middle panel: A frontal view of the image plane is represented before (top) and after (bottom) rotation. Right panel: A top view (*x*–*z*) of the checkerboard is depicted before and after rotation.

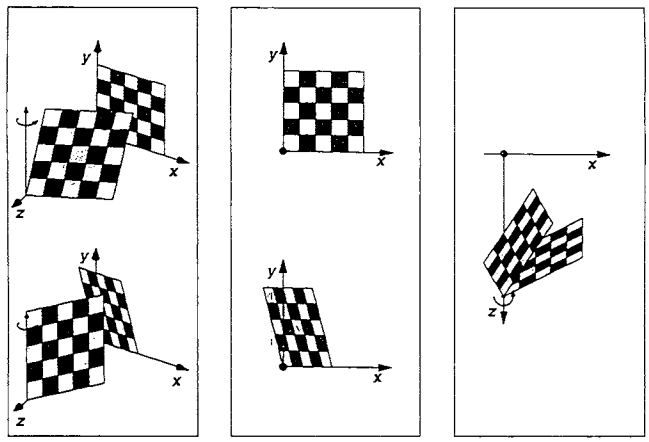

Figure 8. Left panel: A checkerboard plane not parallel to the *y*-axis. The checkerboard is represented before (top) and after (bottom) 30° of rotation about an axis parallel to the *y*-axis. The checkerboard has been predeformed so that, before rotation, each surface element projects on the image plane as a square (on the checkerboard the surface elements are shaped as parallelograms). The figure depicts both the checkerboard (front) and its orthogonal projection on the (*x*–*y*) image plane (back). Middle panel: A frontal view of the image plane is represented before (top) and after (bottom) rotation. Right panel: A top view (*x*–*z*) of the checkerboard is depicted before and after rotation.

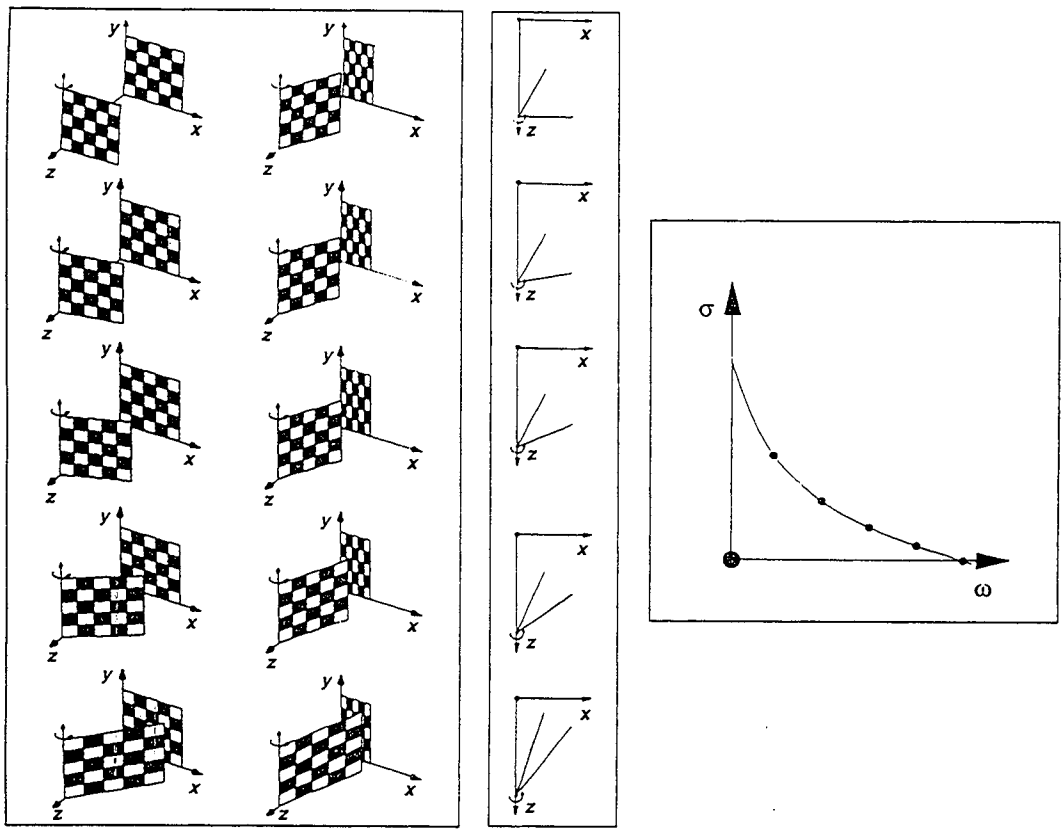

Figure 9. Left panel: Five checkerboards parallel to the *y*-axis are depicted before (left) and after (right) rotation about an axis parallel to the *y*-axis. The checkerboards have been predeformed so that, before rotation, each surface element projects on the image plane as a square. The figure depicts both the checkerboards (front) and their orthogonal projections on the (*x*–*y*) image plane (back). Middle panel: Top views (*x*–*z*) of the checkerboards before and after rotation. The initial orientation of the checkerboards and the magnitudes of angular rotation have been chosen so as to produce the same amount of horizontal compression in the (*x*–*y*) image plane. Right panel: The plot represents a subset of the infinite possible combinations of slant and angular rotation compatible with the 2-D transformations used in this example. The *x*-axis represents the magnitude of angular rotation and the *y*-axis the magnitude of initial slant. The dots correspond to the five combinations of slant and rotation shown in the left panel.

projected slant when the rotatory component is assumed to be zero. On the other hand, Equation 7 shows that *def* is not informative about projected slant when V_{ut} is equal to zero. Nevertheless, we hypothesize that the perceptual system assumes that the relationship between *def* and projected slant also holds when the velocity field is ambiguous, that is, when the velocity field reduces to pure *def*.

In previous research, in fact, we found that *def* is responsible for systematic misperceptions in a variety of psychophysical tasks for which a veridical performance would require the use of the second temporal derivatives of the optic flow. Domini, Caudek, and Proffitt (1997) studied the perceptual discrimination of rigid and nonrigid motion. They found that displays with a low variance of the deformation of the individual triplets of image features[2] tended to be judged as rigid, and those with a high variance of the deformation tended to be judged as nonrigid, regardless of whether they simulated a mathematically correct projection of a rigid motion or not. In another set of experiments, Domini et al. found that, in both two-view and multiview displays, the manipulation of *def* also influenced the magnitude of perceived angular rotation. Regardless of the magnitudes of simulated angular rotation (in multiview displays), perceived rotation was found to be a monotonically increasing function of *def*. Domini, Caudek, Turner, and Favretto (1998) investigated accuracy in the discrimination of constant and variable angular velocities. They found that the judgments of "constant" or "variable" angular velocity were only slightly influenced by the projected angular velocities but were greatly affected by the variations of *def*. When observers viewed a rotating ellipsoidal volume that accelerated and decelerated over the course of rotation,

[2] A triplet of image feature in a two-view sequence provides the minimum conditions for computing *def* (see Domini et al., 1997).

their tendencies to report a variable angular velocity were increased when the acceleration was temporally phased to increase the median *def;* and these tendencies were decreased when the same acceleration pattern was phased to decrease the median *def.* When observers viewed a rotating plane, if the simulated angular velocity varied, there was a slight increase in the tendency to report a varying angular velocity; but if *def* varied, there was a significant increase in the tendency to report a varying angular velocity. Caudek and Domini (1998) investigated the perceived orientation of axis of rotation and observers' accuracy in discriminating fixed-axis from nonfixed-axis rotations. They found that the slant of the axis of rotation (i.e., the angle between the axis and the line of sight) was systematically misperceived. In both two-view and multiview displays, the perceived slant of the axis of rotation was influenced by the ratio between *def* and the component of the global velocity vector parallel to the image plane. If this ratio was kept constant in each frame transition of the stimulus sequence (or if it was varied), then the stimuli tended to be judged as fixed-axis rotations (or as nonfixed-axis rotations) regardless of whether they simulated a fixed-axis rotation or not.

Overview of Experiments

In the following experiments our intent was to extend these previous findings by investigating the relation between *def* and perceived slant in pure *def* velocity fields. Even though several other sources of information have been found to influence perceived surface slant (Flock, 1964, 1965; R. B. Freeman, 1966; Kraft & Winnick, 1967; Olson, 1974), we restricted the present research to the study of the perceptual effects of *def* in stimulus displays in which all other sources of information were controlled. In the following experiments we measured perceived slant in random-dot displays while we independently varied simulated slant (σ) and *def.* Because *def* is equal to the product of σ and ω, Equation 7 can be written as

$$def = \sigma \frac{\Delta\alpha}{N_{\text{frames}}\text{SOA}}, \tag{8}$$

where $\Delta\alpha$ is the magnitude of angular rotation, N_{frames} is the number of frames of the stimulus sequence, and SOA is the stimulus onset asynchrony. The manipulation of σ and *def,* therefore, was performed by varying N_{frames} (Experiment 1) and SOA and $\Delta\alpha$ (Experiment 2). In the first two experiments we tested the hypothesis that perceived slant (σ') is an increasing function of *def* even for a pure *def* velocity field, in which *def* is in principle not informative about the orientation and the motion parameters of a projected surface. In Experiment 3 we tested the hypothesis that both σ' and ω' are recovered by means of a heuristic analysis based on *def* (as described in the following sections). In Experiment 4 we related our heuristic account to previous related findings. Finally, in Experiment 5, we examined the effect of surface tilt on σ'.

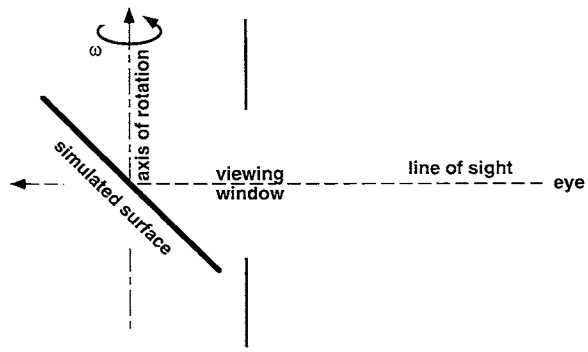

Figure 10. Schematic representation of the planar surfaces simulated in the present experiments. The axis of rotation is parallel to the y-axis and intersects the center of the simulated surface, which corresponds to the center of the viewing window.

General Method

Apparatus. The displays were presented on a high-resolution color monitor (1,280 by 1,024 addressable locations) under the control of a Silicon Graphics IRIS Workstation. The screen had a refresh rate of 60 Hz and was approximately photometrically linearized. An anti-aliasing procedure was used: For point-light locations falling on a pixel boundary, the screen luminance was proportionally adjusted in the relevant addressable locations. The graphics buffer was 8 bits deep (256 gray levels).

Observers viewed the displays through a reduction screen that reduced the field of view to a circular area with a diameter of 9.6° of visual angle. The eye-to-screen distance was 1.1 m. The apparatus was the same in all experiments. Observers viewed the displays with an eyepatch over one of their eyes.

Stimuli. A stimulus display consisted of approximately 100 high-luminance dots moving on a low-luminance background. The motions of the dots simulated an orthographic projection of a planar surface oscillating in 3-D space about an axis in the projection plane. The axis of rotation was positioned in the center of the simulated surfaces (see Figure 10).

Each stimulus display was contained within a circular "window" with a diameter of 9.6° of visual angle; we set the display up this way to prevent changes in the projected contours of the simulated surfaces from being visible. The dots were randomly distributed with uniform probability density over the projection plane (not evenly distributed over the simulated surfaces). A gauge figure was presented in the center of the terminal screen within a circular gap of the stimulus displays. Two different gauge figures (described below) were used (see Figure 11). Movement of a mouse connected to an Iris Workstation varied the represented orientation of the gauge figures.

Procedure. All participants were run individually in one session. They were instructed to manipulate the gauge figure in order to represent the perceived orientation of the simulated surfaces. In Experiment 1 they were also required to represent perceived tilt, and in Experiment 3, perceived angular velocity. The participants were told that the elliptical circumference of the gauge figure should appear as the outline of a circular disc painted on the perceived planar surface.[3] Viewing was monocular, and head and

[3] This method was devised by Koenderink, Van Doorn, and Kappers (1992) for measuring perceived attitude of pictorial depth relief. Because both *def* and σ varied over views, observers were required to report the average perceived slant.

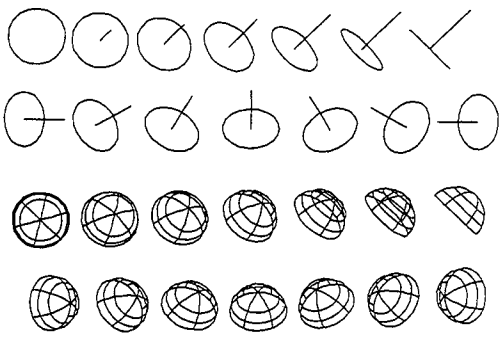

Figure 11. Top two rows: Seven gauge figures used in Experiments 1 and 2. In the top row, tilt is kept constant and slant is varied, whereas in the bottom row, slant is kept constant and tilt is varied. Bottom two rows: Seven hemispheres used in Experiments 3, 4, and 5 for measuring perceived slant and angular velocity. In the top row, tilt is kept constant and slant is varied, whereas in the bottom row, slant is kept constant and tilt is varied.

eye motions were not restricted. The experimental room was dark during the experiment. No restriction was placed on viewing time. No feedback was given until after the experiment was completed.

Experiment 1

In Experiment 1, σ' was measured while *def* and σ were independently varied by manipulating the number of frames of the stimulus sequences and by keeping SOA and rotation magnitude constant (see Equation 8). Because the planar surfaces were simulated as oscillating about an axis passing through their centers (see Figure 10), V_{ut} was equal to zero. As a consequence, the velocity field reduced to a pure *def* which, in principle, was not informative about projected slant (see Equation 7). Nevertheless, also in these circumstances, we hypothesized that σ' would be incorrectly recovered as a monotonic increasing function of *def* by means of a heuristic analysis reminiscent of a motion-parallax interpretation of the first-order optic flow (see Equation 6).

Method

Participants. We (F. D. and C. C.) and 2 naive University of Trieste undergraduates, who volunteered their time, participated in this experiment. All observers had normal or corrected-to-normal vision.

Design. Two variables were studied in this experiment: (a) initial surface slant (0.54, 1.08, 1.62, 2.16, and 2.7, i.e., 28.38°, 47.23°, 58.34°, 65.19°, and 69.71°) and (b) *def* (0.138, 0.225, 0.326, 0.41, and 0.486 rad/s). All variables were within subjects. Each participant viewed four presentations of the 25 conditions in one block, and the order of all trials was completely randomized. Twenty-five additional trials were presented at the beginning of each experimental session for practice.

Stimuli. A planar surface was simulated as oscillating in 3-D space about a vertical axis in the projection plane through an angle of 8°. The tilt of the simulated surfaces was determined randomly on each trial from 0° to 360°. We varied *def* and σ independently by manipulating the number of frames of the stimulus displays and by keeping SOA constant (19.5 ms) and the interstimulus interval (ISI) equal to zero. The number of frames for a stimulus display was computed as (the next integer approximation of) the ratio $N_{\text{frames}} = (\Delta\alpha\sigma/def\text{SOA})$ and varied between 5 and 83 (see Table 1). Given the small angle of rotation, we computed *def* by considering the first and last frames of the stimulus sequence. The axis of rotation was positioned relative to the simulated planar surfaces so as to keep constant the ratio between the maximum and minimum signed 2-D velocities across conditions (see Braunstein et al., 1993).

A gauge figure subtending 3.84° of visual angle (see Figure 11, top two rows) was present in the center of the terminal screen within a circular gap of the stimulus displays. Movement of a mouse connected to an Iris Workstation varied the represented orientation of the gauge figure.

Procedure. Observers were instructed to adjust the gauge figure to report both the perceived tilt and the average perceived slant of the simulated surfaces.

Results and Discussion

The gauge figure settings were broken down into their component slant and tilt directions. Figure 12 shows that both experienced ($\tau' = -4.035 + 1.043\ \tau$, $r^2 = .96$) and naive ($\tau' = -3.771 + 1.058\ \tau$, $r^2 = .92$) observers reported the tilt of the simulated surfaces with high accuracy. This result indicates that observers were able to use the first-order information veridically. Indeed, this information is theoretically sufficient to specify the tilt of the projected surfaces (Hoffman, 1982). We performed a 2 (expertise: experienced vs. naive observers) × 5 (σ: 0.54, 1.08, 1.62, 2.16, and 2.7) × 5 (*def:* 0.138, 0.225, 0.326, 0.41, and 0.486 rad/s) analysis of variance (ANOVA) on the absolute value of the differences between reported and simulated tilt magnitudes to check for any systematic bias in the responses of

Table 1
Stimulus Parameters and Mean Judged Slant in Experiment 1

def (rad/s)	σ	No. of frames	σ'
0.138	0.54	17	0.825
0.138	1.08	33	0.824
0.138	1.62	5	0.841
0.138	2.16	66	0.843
0.138	2.7	83	0.813
0.225	0.54	1	0.868
0.225	1.08	2	0.862
0.225	1.62	3	0.913
0.225	2.16	41	0.918
0.225	2.7	51	0.9
0.326	0.54	7	0.974
0.326	1.08	14	0.983
0.326	1.62	21	0.983
0.326	2.16	28	0.915
0.326	2.7	35	0.942
0.41	0.54	6	0.916
0.41	1.08	11	0.925
0.41	1.62	17	0.983
0.41	2.16	22	0.975
0.41	2.7	28	0.999
0.486	0.54	5	0.95
0.486	1.08	9	1.7
0.486	1.62	14	1.024
0.486	2.16	19	1.011
0.486	2.7	23	0.987

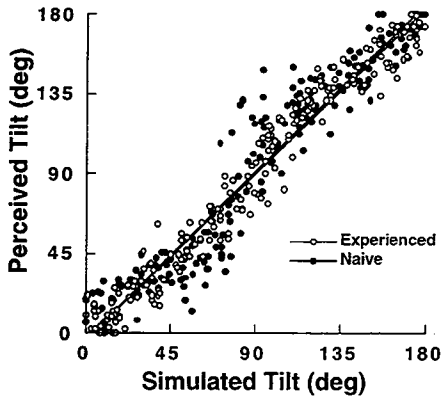

Figure 12. The average judged tilt in Experiment 1 as a function of simulated tilt for experienced and naive observers.

the observers. This analysis, however, did not reveal any significant effect.

Figure 13 shows the plots of σ' versus *def* and σ' versus σ. A 2 (expertise: experienced vs. naive observers) $\times$ 5 (σ: 0.54, 1.08, 1.62, 2.16, and 2.7) $\times$ 5 (*def:* 0.138, 0.225, 0.326, 0.41, and 0.486 rad/s) ANOVA revealed a significant effect of expertise on σ', $F(1, 2) = 52.017$, $p < .05$. Naive observers reported smaller magnitudes of σ' than did experienced observers. Possibly, this result was due to the fact that observers not trained in viewing structure-from-motion displays are less capable of overcoming the flatness cues provided by computer simulations (see, e.g., Proffitt & Kaiser, 1986). The effect of simulated σ was not significant, $F(4, 8) = 0.834$, *ns*. That observers were not sensitive to the projected slant magnitudes theoretically recoverable from the displays (under certain assumptions) may have been due either to the fact that second-order information is not used (or is not used veridically) by the perceptual system or to the fact that in our stimuli the variation of the acceleration field was not large enough (see Hogervorst, Kappers, & Koenderink, 1996). The effect of *def* was significant, $F(4, 8) = 25.986$, $p < .001$. Consistent with our hypothesis, the magnitudes of σ' were a monotonically increasing function of *def*. The interaction between *def* and expertise was also

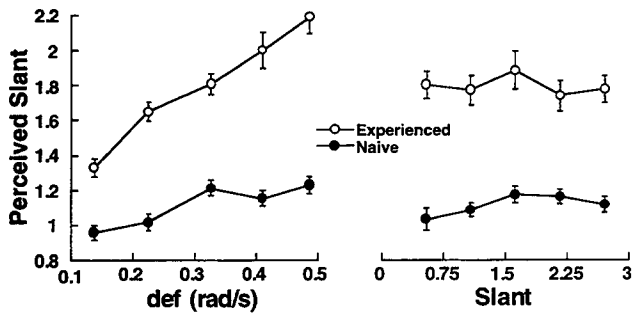

Figure 13. The average judged slant in Experiment 1 as a function of *def* (left panel) and simulated slant (right panel) for experienced and naive observers. Vertical bars represent one standard error.

significant, $F(4, 8) = 7.051$, $p < .01$. Because the mean reported slant was significantly different for experienced and naive observers, this interaction may have been due to the nonlinearity of the tangent function used to transform the data. The interaction between *def* and expertise, in fact, is not significant, $F(4, 8) = 2.35$, *ns*, if the dependent variable is expressed in degrees rather than as the tangent of the perceived angle. None of the remaining interactions was significant.

In conclusion, the results of Experiment 1 indicate that perceived surface attitude is a monotonic function of *def* even though, for a pure *def* velocity field, this component of the first-order optic flow is in principle not informative about projected slant. Therefore, these results support the hypothesis that the perceptual system interprets pure *def* in a heuristic manner by inappropriately relying on the relation between *def* and projected slant, which is appropriate only for a perspective analysis of a linear velocity field when the component V_{ut} is not nil and the rotatory component is zero.

Experiment 2

In Experiment 1, we manipulated *def* by varying the number of frames of the displays. The effect of *def,* therefore, could have been due to the variation of this stimulus parameter. To control for this possible confound, in Experiment 2 we kept the number of frames constant and independently varied σ and *def* by changing the SOA and the magnitude of the simulated rotation.

Method

Participants. We (F. D. and C. C.) and 2 naive University of Trieste undergraduates, who volunteered their time, participated in Experiment 2. The naive observers had not participated in Experiment 1. All observers had normal or corrected-to-normal vision.

Design. Three variables were studied in this experiment: (a) σ (0.54, 1.08, and 1.62, i.e., 28.38°, 47.23°, and 58.34°), (b) *def* (0.074, 0.148, and 0.23 rad/s), and (c) SOA (25, 50, and 100 ms). All variables were within subjects. Each participant viewed four presentations of the 27 different conditions in one block, and the order of all trials was completely randomized. Twenty-seven additional trials were presented at the beginning of each experimental session for practice.

Stimuli. The stimuli were similar to those of Experiment 1 and simulated the orthographic projection of planar surfaces oscillating in 3-D space about a vertical axis contained in the projection plane. The tilt of the simulated surface was randomly selected on each trial and ranged from 0° to 360°. We independently varied *def,* σ, and SOA (with ISI = 0) by keeping constant the number of frames (10) and by changing the magnitude of the total simulated angular rotation ($\Delta\alpha$) according to the following equation:

$$\Delta\alpha = \frac{def N_{\text{frames}} \text{SOA}}{\sigma}.$$

The $\Delta\alpha$ varied between 0.655° and 24.435° (see Table 2).

Procedure. The procedure was the same as that in Experiment 1.

Results and Discussion

As in the previous experiment, the simulated tilt was reported with high accuracy by both experienced

Table 2
Stimulus Parameters and Mean Judged Slant in Experiment 2

def (rad/s)	σ	SOA	Angle of rotation (deg)	σ′
0.074	0.54	25	1.965	1.017
0.074	0.54	50	3.931	1.136
0.074	0.54	100	7.862	1.163
0.074	1.08	25	0.983	1.060
0.074	1.08	50	1.965	1.139
0.074	1.08	100	3.931	1.201
0.074	1.62	25	0.655	1.092
0.074	1.62	50	1.310	1.156
0.074	1.62	100	2.621	1.063
0.148	0.54	25	3.915	1.333
0.148	0.54	50	7.830	1.517
0.148	0.54	100	15.661	1.604
0.148	1.08	25	1.958	1.394
0.148	1.08	50	3.915	1.269
0.148	1.08	100	7.830	1.316
0.148	1.62	25	1.305	1.237
0.148	1.62	50	2.610	1.379
0.148	1.62	100	5.220	1.591
0.230	0.54	25	6.109	1.554
0.230	0.54	50	12.218	1.556
0.230	0.54	100	24.435	1.544
0.230	1.08	25	3.054	1.379
0.230	1.08	50	6.109	1.540
0.230	1.08	100	12.218	1.671
0.230	1.62	25	2.036	1.382
0.230	1.62	50	4.073	1.755
0.230	1.62	100	8.145	1.667

Note. SOA = stimulus onset asynchrony.

($\tau' = -2.27 + 1.02\ \tau$, $r^2 = .95$) and naive ($\tau' = -7.03 + 1.07\ \tau$, $r^2 = .91$) observers. A 2 (expertise: experienced vs. naive observers) × 3 (σ: 0.54, 1.08, and 1.62) × 3 (*def*: 0.074, 0.148, and 0.23 rad/s) × 3 (SOA: 25, 50, and 100 ms) ANOVA on the absolute value of the difference between the reported and simulated tilt magnitudes did not reveal any significant effect.

In Figure 14 are plotted σ′ versus *def* and σ′ versus σ. A 2 (expertise: experienced vs. naive observers) × 3 (σ: 0.54, 1.08, and 1.62) × 3 (*def*: 0.074, 0.148, and 0.23 rad/s) × 3 (SOA: 25, 50, and 100 ms) ANOVA on σ′ revealed a significant effect of expertise, $F(1, 2) = 28.945$, $p < .05$. As in Experiment 1, naive observers reported smaller magnitudes of σ′ than did experienced observers. *Def* significantly affected σ′ $F(2, 4) = 18.358$, $p < .01$; larger magnitudes of σ′ were associated with larger magnitudes of *def*. As in the previous experiment, σ did not significantly affect σ′, $F(2, 4) = 0.503$, *ns*. Neither the effect of SOA nor any of the interactions was significant.

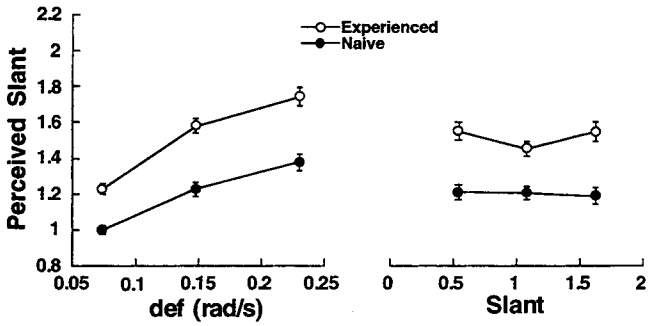

Figure 14. The average judged slant in Experiment 2 as a function of *def* (left panel) and simulated slant (right panel) for experienced and naive observers. Vertical bars represent one standard error.

In conclusion, the results of Experiment 2 replicated those of Experiment 1 even when the number of frames was kept constant and *def* and σ were independently varied by manipulation of the amount of simulated rotation. Also in this experiment, the observers were not able to make veridical use of the second-order temporal information provided by the stimulus displays, and σ′ was systematically influenced by *def* even when *def* was in principle not informative about projected slant.

Heuristic Recovery of Slant and Angular Velocity From Deformation

The results of Experiments 1 and 2 indicate that the perceptual system reliably associates specific magnitudes of σ′ with specific magnitudes of *def* even if pure *def* is ambiguous (i.e., it is compatible with a one-parameter family of different combinations of σ and ω). This then raises the question of how it is possible for the perceptual system to select one out of the infinite possible surface attitude interpretations allowed by pure *def*. The hypothesis that we put forward is that the perceptual system associates surface attitude with *def* by means of a heuristic analysis based on a maximum likelihood criterion (a more general approach to the problem of providing a maximum likelihood interpretation for ambiguous image information has been proposed by W. T. Freeman [1994], who developed a model based on a generic viewpoint assumption for finding the most likely 3-D shape for a given 2-D luminance pattern). Even though *def* is ambiguous when V_{ut} is equal to zero, in fact, not all the σ, ω pairs are equally likely to have produced a given *def* magnitude. In Appendix B it is shown that if one assumes that σ and ω have a priori uniform probability density functions[4] varying between zero and a maximum value, then the conditional probability density function of each σ, ω pair given *def*, $p(\sigma, \omega | def)$, can be calculated. We assume σ and ω have uniform probability density functions because this is the simplest hypothesis in the absence of any a priori knowledge. The distribution of ω is assumed to be bounded by a maximum value because of the limited sensitivity of a biological system. Moreover, because ω is usually induced by the relative movement of the observer with respect to the environment, the maximum value of ω is determined by the maximum velocity of human locomotion.

[4] The use of uniform probability density functions represents a simplifying assumption that we used to develop the simplest model deriving from our assumptions. Other probability density functions may be used, but for the present purposes they are not necessary because this simplified model provides a satisfactory fit of our data.

The distribution of σ is assumed to be bounded by a maximum value because of a geometrical constraint of our displays. When a plane is viewed through an aperture that occludes its edges (as in the present experiments), then in polar projection the maximum slant of a simulated surface cannot be larger than the angle between the image plane and the line connecting the vantage point with the edge of the viewing window.

On the basis of the previous assumptions, it is shown in Appendix B that the maximum value of $p(\sigma, \omega|def)$ is associated with the σ^*, ω^* pair for which

$$\sigma^* = \frac{1}{k}\sqrt{def} \tag{9}$$

$$\omega^* = k\sqrt{def}. \tag{10}$$

According to the previous considerations, therefore, we hypothesize that the human perceptual system recovers the perceived surface attitude and angular velocity magnitudes from pure *def* by choosing the σ, ω pair that maximizes $p(\sigma, \omega|def)$, that is, the σ^*, ω^* pair defined by Equations 9 and 10. We tested this hypothesis in Experiment 3.

Experiment 3

In Experiments 1 and 2 we found that the reported slant magnitudes were a monotonic increasing function of *def*. The heuristic described by Equations 9 and 10, however, identifies a specific pattern of solutions within the one-parameter family of σ, ω pairs compatible with each given *def*. The present experiment was designed to measure both σ' and ω' for four selected *def* magnitudes so that the perceived values could be compared with the solutions identified by Equations 9 and 10.

Method

Participants. There were 14 observers who constituted two groups: a naive group composed of 12 University of Trieste undergraduates who were naive to the purpose of the experiment and an experienced group composed of the two of us (F. D. and C. C.). The naive observers, who volunteered their time, had not participated in any of the previous experiments. All observers had normal or corrected-to-normal vision.

Design. Two dependent variables were measured: perceived surface attitude and angular velocity. The independent variables were σ (1.125, 1.75, 2.375, and 3, i.e., 48.39°, 60.28°, 67.2°, and 71.6°) and *def* (0.097, 0.873, 1.648, and 2.424 rad/s). All variables were within subjects. Each participant viewed one presentation of the 16 conditions in one session, and the order of all trials was completely randomized. To familiarize the observers with the stimulus displays, we presented 16 additional trials at the beginning of each experimental session.

Stimuli. We independently manipulated σ and *def* by varying the magnitude of simulated rotation ($\Delta\alpha$); $\Delta\alpha$ varied between 0.55° and 36.688° (see Table 3). The number of frames in each stimulus sequence was kept constant (10), the SOA was 33 ms, and the ISI was 0. We computed *def* by considering the first and second frames of the stimulus sequence.

Table 3
Stimulus Parameters, Mean Judged Slant, and Mean Judged Angular Velocity in Experiment 3

def (rad/s)	σ	Angle of rotation (deg)	σ'	ω' (rad/s)
0.097	1.125	1.467	0.54	0.277
0.097	1.75	0.943	0.634	0.201
0.097	2.375	0.694	0.682	0.275
0.097	3	0.55	0.415	0.206
0.873	1.125	13.208	1.635	0.916
0.873	1.75	8.49	1.392	0.775
0.873	2.375	6.256	1.287	0.833
0.873	3	4.953	1.091	0.934
1.648	1.125	24.948	1.157	1.216
1.648	1.75	16.038	1.316	1.264
1.648	2.375	11.817	1.869	1.169
1.648	3	9.355	1.379	1.376
2.424	1.125	36.687	1.881	1.484
2.424	1.75	23.584	1.939	1.45
2.424	2.375	17.378	1.55	1.475
2.424	3	13.758	1.333	1.705

To increase the salience of foreshortening information, we modified the gauge figure used in the previous experiments. On each trial, an oscillating transparent hemisphere made up of three equally spaced "meridians" and three "parallels" (see Figure 11, bottom two rows) was presented on the central part of the monitor screen within a circular gap of the stimulus display. The hemisphere subtended 3.84° of visual angle and oscillated in phase with the stimulus displays about a vertical axis. Observers could vary the slant of its base and its amplitude of rotation in real time by using a mouse connected to an Iris Workstation. The initial slant and the initial 3-D angular velocity of the hemisphere were randomly selected on each trial. The tilt of the base of the hemisphere was set to be equal to the tilt of the simulated surfaces.

Procedure. The observers were instructed to manipulate the slant and the angular velocity of the hemisphere so that its base appeared to be parallel to the random-dot surface for the whole duration of each oscillation cycle. The adjusted slant and angular velocity of the hemisphere associated with the first two frames of the apparent motion sequence served as the input for the following analyses.

Results and Discussion

The data of the naive and experienced observers were analyzed separately. For the data of the naive observers, a preliminary multivariate analysis of variance (MANOVA) was performed on the two dependent variables (σ' and ω') with *def* as the independent variable. With the use of Wilks's criterion, this analysis showed that the combined dependent variables were significantly affected by the square root of *def*, $F(6, 86) = 16.874$, $p < .001$, $\eta^2 = .83$.

We performed a direct test of the proposed heuristic by comparing the mean σ' and ω' magnitudes in each of the 16 cells of the factorial design with the predictions of Equations 9 and 10. We used an iterative procedure to find the constant k of Equations 9 and 10, which minimizes the squared differences between the observed and the predicted scores for each observer. An overall measure of fit of the model on the average settings reported by the naive observers was

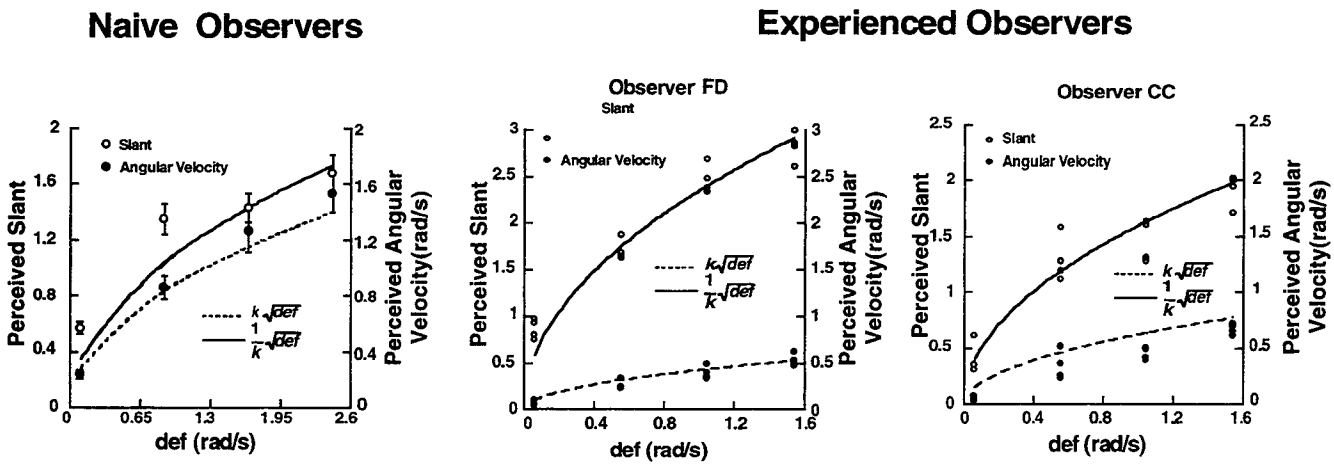

Figure 15. Left panel: Mean judged slant and angular velocity as a function of *def* together with the predictions of Equations 9 and 10 (black and dotted lines) in Experiment 3 for the naive observers. Middle and right panels: Raw data of experienced observers F. D. and C. C. plotted together with the predictions of Equations 9 and 10.

calculated as

$$\frac{1}{4}\sum_{i=1}^{4}\frac{\sqrt{e_\sigma^2 + e_\omega^2}}{\sqrt{\hat{\sigma}^2 + \hat{\omega}^2}}.$$

This measure was equal to .21, and it can be interpreted as an average error of 21% in the predictions. For the naive observers, Figure 15 (left panel) shows the reported mean σ' and ω' magnitudes as a function of *def*, together with the predictions of Equations 9 and 10. Figure 16 (left panel) shows the σ' and ω' pairs corresponding to the four simulated *def* magnitudes plotted in the σ, ω space, together with the predictions of Equations 9 and 10. If $\sigma' = (1/k)\sqrt{def}$ and $\omega' = k\sqrt{def}$, then the predicted σ, ω pairs lie on the line $\sigma = (1/k^2)\omega$.

The reasonable fit of the proposed heuristic can be contrasted with the absence of any significant relation between σ' and σ. When simulated slant was used as the independent variable, in fact, the R for regression for the naive observers was not significantly different from zero, $F(1, 14) = 0.428$, *ns*.

The pattern revealed by the averaged data was confirmed by the analysis of the complete data set of each observer. We

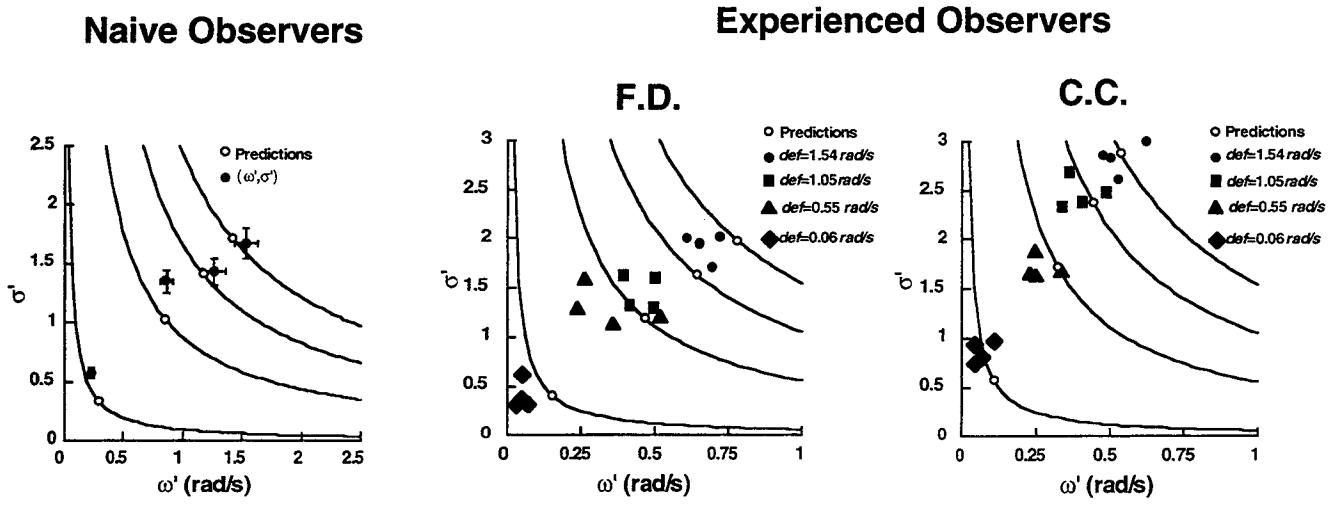

Figure 16. Left panel: Mean judged slant and angular velocity (filled circles) together with the predictions of Equations 9 and 10 in the σ, ω space (open circles) for the four *def* magnitudes of Experiment 3 for the naive observers. The hyperbolas represent the loci of the σ, ω pairs compatible with the *def* magnitudes used in the experiment. Middle and right panels: Raw data of experienced observers F. D. and C. C. plotted in the σ, ω space together with the predictions of Equations 9 and 10.

performed two separate regression analyses for each observer on the perceived surface attitude and angular velocity magnitudes by using the predictions of Equations 9 and 10 as the independent variable. A summary of these analyses is reported in Table 4.

An examination of the r^2 values reported in Table 4 reveals, however, that a considerable portion of the variance of the judgments of the naive observers is not accounted for by the proposed model. This unexplained variability may be attributed to two different causes: (a) the influence of other variables not considered by Equations 9 and 10 and (b) the limited training in structure-from-motion tasks.

Perotti and Todd (in press) suggested that among the possible variables influencing perceived surface attitude, a plausible candidate may be surface tilt. To check for this possible orientation anisotropy, we performed two new regression analyses on the complete data set of the naive observers by using perceived slant and angular velocity as dependent variables and simulated tilt as the independent variable. Both of these analyses produced a significant result, thus confirming that perceived surface attitude is also influenced by simulated tilt: $\sigma' = 1.0 + .33$ tilt, $r^2 = .04$, $F(1, 190) = 6.92$, $p < .01$; $\omega' = 1.25 - .36$ tilt, $r^2 = .05$, $F(1, 190) = 11.14$, $p < .01$.

Table 4
Regression Values for Experiment 3

Observers	Slope	y intercept	r^2
Perceived surface attitude			
Naive			
Al.	.64	.57	.27
El.	.74	.26	.36
Fi.	.55	.88	.10
Ig.	1.14	.07	.26
Ju.	.59	.50	.18
Ka.	.60	.52	.11
Lo.	.69	.29	.30
Lu.	.32	.83	.22
Me.	.85	.21	.33
Mi.	1.01	.12	.46
Ni.	1.32	.05	.38
Pa.	.85	.16	.55
Experienced			
F.D.	.86	.32	.97
C.C.	.91	.07	.91
Perceived angular velocity			
Naive			
Al.	1.05	.04	.76
El.	.56	.39	.29
Fi.	1.54	−.25	.87
Ig.	1.25	−.37	.64
Ju.	1.03	−.04	.57
Ka.	1.11	−.10	.57
Lo.	.76	−.04	.50
Lu.	.98	−.14	.58
Me.	1.24	−.26	.63
Mi.	1.45	−.17	.41
Ni.	1.88	−.19	.77
Pa.	.77	.05	.53
Experienced			
F.D.	1.08	−.06	.89
C.C.	.92	−.10	.89

In light of this result, we decided to collect a new set of data. We used the experimental design previously described, but we set simulated tilt equal to 90° in all trials. We (F. D. and C. C.) served as the only observers. In this experiment the SOA was equal to 52 ms. Figure 15 (right panel) shows the reported σ' and ω' magnitudes as a function of *def*, together with the predictions of Equations 9 and 10. Figure 16 (right panel) shows the σ' and ω' pairs corresponding to the four simulated *def* magnitudes plotted in the σ, ω space, together with the predictions of Equations 9 and 10. For the experienced group, the fit of the model calculated on the complete data set of each observer was equal to .18 and .21, respectively, for F. D. and C. C. The results of the regression analyses predicting perceived surface attitude and angular velocity magnitudes from Equations 9 and 10 are reported in Table 4.

The comparison between the naive and experienced groups indicates that (a) the data show the same trend in both groups and (b) when surface tilt is controlled and sufficient training in a structure-from-motion task is provided, the predictions of the heuristic model described by Equations 9 and 10 account for a large proportion of the variance of the perceived surface attitude and angular velocity magnitudes.

In conclusion, the results of Experiment 3 support the hypothesis that specific magnitudes of surface slant and angular velocity are perceptually recovered from an ambiguous pure *def* velocity field according to the heuristic model described by Equations 9 and 10. The results also indicate, however, that perceived surface attitude is also in part influenced by simulated tilt. The effect of simulated tilt on perceived surface attitude is not accounted for by the proposed heuristic and is further examined in Experiment 5.

Experiment 4

Previous related investigations (Loomis & Eby, 1988; Todd & Norman, 1991) have shown that the manipulation of simulated angular velocity has a negligible effect on perceived surface attitude compared with the manipulation of simulated surface slant. These findings seem to be in contrast to the proposed heuristic because, according to Equations 9 and 10, simulated slant and angular velocity should have the same influence on perceived surface attitude. Therefore, we must more closely examine these results, which seem to be inconsistent with the predictions of our model.

Loomis and Eby (1988) simulated half-ellipsoids (oriented with their axes normal to the image plane) simultaneously rotating about their main axes and revolving in the image plane. They varied the simulated depth of the half-ellipsoids and their angular velocity and found that the manipulation of simulated depth had a larger effect on perceived depth than did the manipulation of angular velocity. We should note, however, that in their displays the first-order properties of the velocity field were affected differently by the manipulation of simulated depth and by the manipulation of angular velocity. The manipulation of

simulated depth produced a small change in the average 2-D velocity and a large change in the magnitude of *def*. On the other hand, the manipulation of angular velocity had comparable effects on *def* and average 2-D velocity. The results of Loomis and Eby, therefore, are consistent with a motion-parallax interpretation of the optic flow. According to Equation 6, in fact, we should expect that the manipulation of simulated depth would influence the recovered slant magnitudes more than would the manipulation of angular velocity.

A similar result was reported by Todd and Norman (1991). They simulated the orthographic projection of a sinusoidally corrugated surface rotating in depth about an axis parallel to the direction of maximum curvature. Todd and Norman manipulated both the peak-to-through amplitude of the corrugations and angular velocity. In their stimuli, the amplitude of the corrugations can be interpreted as the average slant of one of the sides of a corrugation. Todd and Norman found that the increase of the simulated amplitude of the corrugations influenced the perceived amplitude of the corrugations or, in other words, perceived slant. However, a corresponding increase in the simulated angular velocity produced only a negligible effect on perceived slant. Also in this case, however, the first-order properties of the velocity field were affected differently by the manipulation of the simulated amplitude of the corrugations and by the manipulation of angular velocity. For the stimuli of Todd and Norman, the manipulation of the simulated amplitude of the corrugations varied the magnitude of *def* while leaving unchanged average 2-D velocity. Conversely, the manipulation of simulated angular velocity produced a comparable variation in the magnitudes of both *def* and average 2-D velocity. Also in this case, therefore, the negligible effect of angular velocity on perceived slant is consistent with a motion-parallax analysis of the optic flow. According to Equation 6, in fact, we should expect that the manipulation of the simulated amplitude of the corrugations would have a larger effect on the recovered slant magnitudes than would the manipulation of angular velocity.

The previous findings, therefore, suggest that a sort of motion-parallax analysis was performed by Loomis and Eby's (1988) and Todd and Norman's (1991) observers, even though the stimulus displays were generated by an orthographic projection. This interpretation is supported by the fact that in both of these previous reports, perceived slant was proportional to *def* and inversely proportional to the average 2-D velocity (see Equation 6). The hypothesis that the perceptual interpretation of the first-order optic flow is consistent with a motion-parallax analysis has also been proposed by Braunstein et al. (1993).

The previous reports indicating that the manipulation of simulated angular velocity has a negligible effect on perceived slant (compared with the effect of the manipulation of simulated slant) may be reconciled with the predictions of our heuristic model by restricting the scope of the model: We propose that Equations 9 and 10 describe the heuristic recovery of perceived surface attitude (and perceived angular velocity) from a linear velocity field only when the variations of *def* leave average 2-D velocity unchanged. In such a case, in fact, the variation of simulated slant influences the first-order properties of the optic flow in exactly the same manner as does a comparable variation of simulated angular velocity (the manipulation of these two variables, however, has different effects on the temporal properties of the second-order optic flow). To test the previous hypothesis, we designed Experiment 4 to measure the relative influence of simulated angular velocity and simulated slant on perceived surface attitude in stimulus displays in which the manipulation of these variables did not vary average 2-D velocity. In these particular stimulus conditions, we expected that comparable variations of σ and ω would have the same effect on perceived surface attitude.

Method

Participants. Five naive University of Trieste undergraduates, who volunteered their time, participated as observers in this experiment. They had not participated in any of the previous experiments. All observers had normal or corrected-to-normal vision.

Design. The within-subjects independent variables were σ (1.5 and 3.0, i.e., 56.34° and 71.6°) and ω (0.25 and 5.0 rad/s). Each observer viewed four presentations of the four conditions in one session, and the order of all trials was completely randomized. We presented 16 additional trials at the beginning of each experimental session to familiarize the observers with the stimulus displays.

Stimuli. Planar surfaces with a tilt of 90° were simulated as oscillating through an angle of 8° or 16° about the *y*-axis. The number of frames in each stimulus sequence was 20, the SOA was 28 ms, and the ISI was 0. The same gauge figure used in Experiment 3 was used in this experiment.

Procedure. The procedure was the same as that in Experiment 3.

Results and Discussion

Figure 17 shows the plots of σ' versus σ. A 2 (angular velocity: 0.25 and 5.0 rad/s) × 2 (σ: 1.5 and 3.0) within-subjects ANOVA revealed significant effects of both angular velocity, $F(1, 4) = 20.22$, $p < .05$, and slant, $F(1, 4) = 21.29$, $p < .01$, on σ'. Both variables had a comparable effect on σ': When simulated angular velocity was doubled,

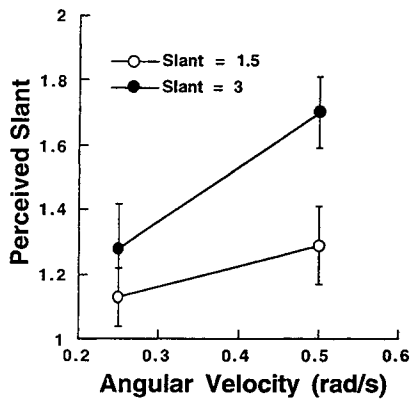

Figure 17. The average judged slant in Experiment 4 as a function of simulated angular velocity for two simulated slant magnitudes. Vertical bars represent one standard error.

σ' increased by 24%; when simulated slant was doubled, σ' increased by 23%. The interaction between slant and angular velocity was not significant, $F(1, 4) = 3.78$, *ns*.

In conclusion, the results of the present experiment support the hypothesis that when the manipulation of *def* leaves 2-D average velocity unchanged (as in the case of pure *def*), the manipulation of simulated angular velocity and the manipulation of simulated slant affect perceived surface attitude in a similar manner. These results, therefore, are consistent with the heuristic model of the recovery of surface attitude from pure *def* that is described by Equations 9 and 10.

Experiment 5

Our purpose in Experiment 5 was to examine more closely the orientation anisotropies revealed by Experiment 3. Previous reports of orientation anisotropies in structure from motion were provided by Rogers and Graham (1983) and Cornilleau-Peres and Droulez (1989). Rogers and Graham reported that cylinders that were curved in a direction orthogonal to the axis of rotation were more perceptually salient than were those curved in a direction parallel to the axis of rotation. Similarly, Cornilleau-Peres and Droulez found that a cylinder/plane discrimination was more accurate for rotations about an axis orthogonal to the cylinder's principal axis. Similar results were also reported by Norman and Lappin (1992), Norman and Todd (1995), and Perotti and Todd (in press). In the present experiment we examined the influence of surface tilt on σ' by manipulating surface tilt for two simulated *def* magnitudes.

Method

Participants. Seven naive University of Trieste undergraduates, who volunteered their time, participated as observers in this experiment. They had not participated in any of the previous experiments. All observers had normal or corrected-to-normal vision.

Design. The within-subjects independent variables were tilt (0°, 30°, 60°, and 90°) and *def* (0.337 and 0.674 rad/s). Each observer viewed four presentations of the eight conditions in one session, and the order of all trials was completely randomized. We presented 16 additional trials at the beginning of each experimental session to familiarize the observers with the stimulus displays.

Stimuli. We manipulated *def* by changing the angle of rotation, which took on the values of 4° and 8°. The number of frames in each stimulus sequence was 30, the SOA was 28 ms, and the ISI was 0. The same gauge figure used in Experiment 3 was also used in this experiment.

Procedure. The procedure was the same as that in Experiment 3.

Results and Discussion

Figure 18 shows the plots of σ' versus tilt as a function of *def*. A 4 (tilt: 0°, 30°, 60°, and 90°) × 2 (def: 0.337 and 0.674 rad/s) within-subjects ANOVA revealed a significant effect of tilt, $F(3, 18) = 9.19$, $p < .01$. The variable *def* was also significant, $F(1, 6) = 12.59$, $p < .05$, whereas the interaction between tilt and *def* was not, $F(3, 18) = 1.03$, *ns*. These results, therefore, replicate the findings of Experiment 3. Also in this experiment we found that by keeping everything else constant, perceived surface attitude increased as surface tilt varied from 0° to 90°. This result confirms the previously reported findings that a velocity gradient is more perceptually salient when it is parallel to the axis of rotation.

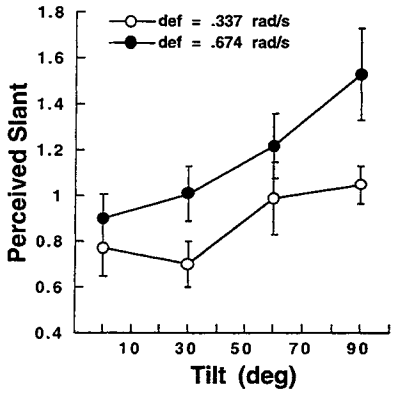

Figure 18. The average judged slant in Experiment 5 as a function of simulated surface tilt for two simulated *def* magnitudes. Vertical bars represent one standard error.

General Discussion

Previous research has shown that perceived surface attitude in motion-parallax displays is strongly affected by *def*, one of the properties of the first-order velocity field. T. C. A. Freeman, Harris, and Meese (1995), for example, found that the addition (or subtraction) of a *def* component to a velocity field produced by the perspective projection of a horizontally translating surface gives rise to a predictable increase (or decrease) in the perceived slant magnitudes. In the present article we have considered the simplest velocity field, that is, the linear velocity field. In the introduction we distinguished between the case in which a common motion component V_{ut} is present in the velocity field and the case in which it is not. If a common motion component V_{ut} is present, then a perspective analysis assuming a nil rotatory component can veridically recover projected slant from a linear velocity field (because projected slant is proportional to the ratio between *def* and V_{ut}). If a common motion component V_{ut} is absent, on the other hand, projected slant cannot be veridically recovered. In these conditions, in fact, the velocity field reduces to pure *def* and therefore is ambiguous. We designed the present research to study the perceptual recovery of surface attitude from an ambiguous pure *def* velocity field. In these circumstances, we found that perceived surface attitude was strongly influenced by *def*, whereas projected slant was not found to have any significant effect.

The present results, therefore, do not support the view that the perceptual recovery of surface slant is carried out consistently with a geometrically correct analysis of the second-order temporal relations of the optic flow. In fact, even when our multiview displays provided information

theoretically sufficient (under certain assumptions) for a veridical derivation of the projected surface attitude, this information was not used, or it was used incorrectly. Although many researchers agree that computer vision algorithms based on second-order temporal relations do not provide adequate models for human vision (e.g., Braunstein, 1976, 1994; Braunstein & Andersen, 1984; Caudek & Proffitt, 1993; Domini & Braunstein, 1998; Domini et al., 1997; Liter, Braunstein, & Hoffman, 1993; Pollick, Nishida, Koike, & Kawato, 1994; Ramachandran, 1985), the issue of how perceived surface slant is derived from the optic flow is still debated.

In this regard we propose that when the velocity field reduces to pure *def*, the perceptual recovery of surface attitude may be understood as a heuristic process based on a maximum-likelihood criterion. In Appendix B, in fact, we show that, under certain assumptions, not all possible σ, ω pairs are equally likely to have produced a given *def*. For σ and ω magnitudes coming from square probability distributions, for example, the conditional probability of a σ, ω pair given *def* is given by Equation B1. Consistent with this analysis is our hypothesis that the perceptual system also recovers σ' and ω' from *def* by determining the σ, ω pair that is associated with the maximum conditional probability for the *def* component of the velocity field. The data of the present research support this hypothesis. In fact, we found that the magnitudes of both σ' and ω' were well accounted for by the predictions of Equations 9 and 10.

Our heuristic model, however, does not completely explain the perceptual recovery of surface attitude from pure *def*. In fact, we found that perceived surface attitude is also affected by surface tilt, and this orientation anisotropy is not predicted by our model. Orientation anisotropies have been reported previously in the structure-from-motion literature (Cornilleau-Peres & Droulez, 1989; Norman & Lappin, 1992; Norman & Todd, 1995; Perotti & Todd, in press; Rogers & Graham, 1983). Consistent with these previous reports is our finding that perceived slant magnitudes increase as tilt increases from 0° to 90°.

Our results relating judged surface slant to *def* are consistent with the results of a recent investigation on the relation between judged shape of a dihedral angle and the velocity gradients in orthogonal directions (Liter & Braunstein, 1998). Liter and Braunstein simulated dihedral angles consisting of two planes slanted about a horizontal axis and meeting at a horizontal edge, and they examined both perspective projections of translations (with the dihedral edge either frontal parallel or rotated about the vertical axis) and orthographic projections of rotations about a vertical axis. In order to relate their results to our heuristic account, we computed *def* for the slanted planes comprising the dihedral angles in each condition in their study and transformed judged shape magnitudes into slant magnitudes (assuming perceived tilt equal to simulated tilt). Mean values of *def* were used for the rotated translations and rotations, because *def* varied over views for these conditions. *Def* magnitudes had the smallest value for the frontal translations and larger and similar values for rotated translations and rotations. Consistent with our heuristic account is Liter and Braunstein's finding that perceived slant magnitudes had the smallest values for frontal translations and larger and similar values for rotated translations and rotations. Liter and Braunstein also found that the rotations and the rotated translations were judged as undergoing greater angular displacements than were the frontal translations, although in fact the rotated translations, like the frontal parallel translations, displayed a null angular displacement. These results are also consistent with our heuristic account because we propose that the perceived amount of rotation is an increasing function of *def*.

In conclusion, the present investigation indicates that for projections of rotating planar surfaces producing a pure *def* velocity field, rather than correctly analyzing the second-order temporal derivatives of the velocity field, the perceptual system associates greater values of slant and angular velocity with greater values of *def* regardless of the simulated slant and angular velocity magnitudes. These systematic misperceptions are consistent with a heuristic analysis of the first-order optic flow that is based on a maximum-likelihood criterion, even though residual orientation anisotropies are present that are not accounted for by our heuristic model.

References

Bennett, B. M., Hoffman, D. D., Nicola, J. E., & Prakash, C. (1989). Structure from two orthographic views of rigid motion. *Journal of the Optical Society of America, A6,* 1052–1069.

Braunstein, M. L. (1962). Depth perception in rotating dot patterns: Effects of numerosity and perspective. *Journal of Experimental Psychology, 64,* 415–420.

Braunstein, M. L. (1966). Sensitivity of the observer to transformations of the visual field. *Journal of Experimental Psychology, 72,* 683–689.

Braunstein, M. L. (1968). Motion and texture as sources of slant information. *Journal of Experimental Psychology, 78,* 247–253.

Braunstein, M. L. (1976). *Depth perception through motion.* New York: Academic Press.

Braunstein, M. L. (1994). Decoding principles, heuristics and inference in visual perception. In G. Johansson, S. S. Bergstrom, & W. Epstein (Eds.), *Perceiving events and objects* (pp. 436–446). Hillsdale, NJ: Erlbaum.

Braunstein, M. L., & Andersen, G. (1981). Velocity gradients and relative depth perception. *Perception & Psychophysics, 29,* 145–155.

Braunstein, M. L., & Andersen, G. (1984). A counterexample to the rigidity assumption in the visual perception of structure from motion. *Perception, 13,* 213–217.

Braunstein, M. L., Liter, C. J., & Tittle, J. S. (1993). Recovering three-dimensional shape from perspective translations and orthographic rotations. *Journal of Experimental Psychology: Human Perception and Performance, 19,* 598–614.

Braunstein, M. L., & Tittle, J. S. (1988). The observer-relative velocity field as the basis for effective motion parallax. *Journal of Experimental Psychology: Human Perception and Performance, 14,* 582–590.

Caudek, C., & Domini, F. (1998). Perceived orientation of axis of rotation in structure-from-motion. *Journal of Experimental Psychology: Human Perception and Performance, 24,* 609–621.

Caudek, C., & Proffitt, D. R. (1993). Depth perception in motion

parallax and stereokinesis. *Journal of Experimental Psychology: Human Perception and Performance, 19,* 32–47.

Clocksin, W. F. (1980). Perception of surface slant and edge labels from optical flow: A computational approach. *Perception, 9,* 253–269.

Cornilleau-Peres, V., & Droulez, J. (1989). Visual perception of surface curvature: Psychophysics of curvature detection induced by motion parallax. *Perception & Psychophysics, 46,* 351–364.

Domini, F., & Braunstein, M. L. (1998). Recovery of 3-D structure from motion is neither Euclidean nor affine. *Journal of Experimental Psychology: Human Perception and Performance, 24,* 1273–1295.

Domini, F., Caudek, C., & Proffitt, D. R. (1997). Misperceptions of angular velocities influence the perception of rigidity in the kinetic depth effect. *Journal of Experimental Psychology: Human Perception and Performance, 23,* 1111–1129.

Domini, F., Caudek, C., Turner, J., & Favretto, A. (1998). Discriminating constant from variable angular velocities in structure from motion. *Perception & Psychophysics, 60,* 747–760.

Flock, H. R. (1964). A possible optical basis for monocular slant perception. *Psychological Review, 71,* 380–391.

Flock, H. R. (1965). Optical texture and linear perspective as stimuli for slant perception. *Psychological Review, 72,* 505–514.

Freeman, R. B. (1966). The effect of size on visual slant. *Journal of Experimental Psychology, 71,* 96–103.

Freeman, T. C. A., Harris, M. G., & Meese, T. S. (1995). On the relationship between deformation and perceived surface slant. *Vision Research, 35,* 317–322.

Freeman, W. T. (1994). The generic viewpoint assumption in a framework for visual perception. *Nature, 368,* 542–545.

Graham, M., & Rogers, B. (1982). Simultaneous and successive contrast effects in the perception of depth from motion-parallax and stereoscopic information. *Perception, 11,* 247–262.

Hoffman, D. D. (1982). Inferring local surface orientation from motion fields. *Journal of the Optical Society of America, A72,* 888–892.

Hoffman, D. D., & Bennett, B. M. (1985). Inferring the relative 3-D positions of two moving points. *Journal of the Optical Society of America, A2,* 350–533.

Hoffman, D. D., & Bennett, B. M. (1986). The computation of structure from fixed-axis motion: Rigid structures. *Biological Cybernetics, 54,* 71–83.

Hogervorst, M. A., Kappers, A. M. L., & Koenderink, J. J. (1996). Structure from motion: A tolerance analysis. *Perception & Psychophysics, 58,* 449–459.

Koenderink, J. J. (1986). Optic flow. *Vision Research, 26,* 161–179.

Koenderink, J. J., & Van Doorn, A. J. (1975). Invariant properties of the motion parallax field due to the movement of rigid bodies relative to an observer. *Optica Acta, 22,* 773–791.

Koenderink, J. J., & Van Doorn, A. J. (1976). Local structure of movement parallax of the plane. *Journal of the Optical Society of America, A66,* 717–723.

Koenderink, J. J., & Van Doorn, A. J. (1990). Affine structure from motion. *Journal of the Optical Society of America, A8,* 377–385.

Koenderink, J. J., Van Doorn, A. J., & Kappers, A. M. L. (1992). Surface perception in pictures. *Perception & Psychophysics, 52,* 487–498.

Kraft, A. L., & Winnick, W. A. (1967). The effect of pattern and texture gradient on slant and shape judgements. *Perception & Psychophysics, 58,* 449–459.

Liter, J. C., & Braunstein, M. L. (1998). The relationship of vertical and horizontal velocity gradients in the perception of shape, rotation, and rigidity. *Journal of Experimental Psychology: Human Perception and Performance, 24,* 1257–1272.

Liter, J. C., Braunstein, M. L., & Hoffman, D. D. (1993). Inferring structure from motion in two-view and multiview displays. *Perception, 22,* 1441–1465.

Longuet-Higgins, H. C., & Prazdny, K. (1980). The interpretation of a moving retinal image. *Proceedings of the Royal Society of London,* Series B, *208,* 385–397.

Loomis, J. M., & Eby, D. W. (1988). Perceiving structure from motion: Failure of shape constancy. In *Proceedings of the Second International Conference on Computer Vision* (pp. 383–391). Washington, DC: IEEE Computer Society Press.

Norman, J. F., & Lappin, J. S. (1992). The detection of surface curvatures defined by optical motion. *Perception & Psychophysics, 51,* 386–396.

Norman, J. F., & Todd, J. T. (1995). The perception of 3-D structure from contradictory optical patterns. *Perception & Psychophysics, 57,* 826–834.

Olson, R. K. (1974). Slant judgements from static and rotating trapezoids correspond to rules of perspective geometry. *Perception & Psychophysics, 15,* 509–516.

Ono, M. E., Rivest, J., & Ono, H. (1986). Depth perception as a function of motion parallax and absolute-distance information. *Journal of Experimental Psychology: Human Perception and Performance, 12,* 331–337.

Perotti, V. J., & Todd, J. T. (in press). The visual perception of surface orientation from optical motion. *Perception & Pychophysics.*

Pollick, F. E., Nishida, S., Koike, Y., & Kawato, M. (1994). Perceived motion in structure from motion: Pointing responses to the axis of rotation. *Perception & Psychophysics, 56,* 91–109.

Prazdny, K. (1980). Egomotion and relative depth map from optical flow. *Biological Cybernetics, 36,* 87–102.

Proffitt, D. R., & Kaiser, M. K. (1986). The use of computer graphics animation in motion perception research. *Behavior Research Methods, Instruments, & Computers, 18,* 487–492.

Ramachandran, V. S. (1985). The neurobiology of perception. *Perception, 14,* 1–7.

Rogers, B. J., & Collett, T. S. (1989). The appearance of surfaces specified by motion parallax and binocular disparity. *Quarterly Journal of Experimental Psychology: Human Experimental Psychology, 41A,* 697–717.

Rogers, B., & Graham, M. (1979). Motion parallax as an independent cue for depth perception. *Perception, 8,* 125–134.

Rogers, B., & Graham, M. (1982). Similarities between motion parallax and stereopsis in human depth perception. *Vision Research, 22,* 261–270.

Rogers, B., & Graham, M. (1983). Anisotropies in the perception of three-dimensional surfaces. *Science, 221,* 1409–1411.

Todd, J. T., & Norman, J. F. (1991). The visual perception of smoothly curved surfaces from minimal apparent motion sequences. *Perception & Psychophysics, 50,* 509–523.

Ullman, S. (1979). *The interpretation of visual motion.* Cambridge, MA: MIT Press.

(Appendixes follow)

Appendix A

Perspective Projection of a Moving Planar Surface

Let us consider the coordinate system depicted in Figure 5. A point $P(x, y, z)$ viewed from a vantage point located at $(0, 0, e)$ projects on the image plane a point P' with coordinates (u, v) given by

$$u = \frac{xe}{e - z} \tag{A1}$$

$$v = \frac{ye}{e - z}. \tag{A2}$$

The generic velocity field produced by the projection of a moving point is

$$\dot{u} = \frac{\dot{x}e(e - z) + \dot{x}ze}{(e - z)^2} \tag{A3}$$

$$\dot{v} = \frac{\dot{y}e(e - z) + \dot{y}ze}{(e - z)^2}. \tag{A4}$$

Let us consider the particular case of a velocity field produced by the perspective projection of a planar surface rotating in 3-D space about the y-axis (with angular velocity ω) and translating in a direction parallel to the x-axis (with linear velocity V_x). Without a loss of generality, we can choose a planar surface passing through the origin of the coordinate system. For such a case, the equation of the surface is

$$z = g_1 x + g_2 y, \tag{A5}$$

where g_1 and g_2 are the x, y components of the depth gradient. The 3-D velocity vector of a generic point (x, y, z) of the surface is

$$\dot{x} = (g_1 x + g_2 y)\omega + V_x$$

$$\dot{y} = 0$$

$$\dot{z} = -\omega x. \tag{A6}$$

By substituting Equations A1, A2, A5, and A6 in the general equations of the velocity field (Equations A3 and A4), we obtain

$$\dot{u} = \left(-\frac{\omega}{e}\right)u^2 + (g_1 u + g_2 v)\left(\omega + \frac{V_x}{e}\right) + V_x$$

$$\dot{v} = \left(-\frac{\omega}{e}\right)uv. \tag{A7}$$

In a small neighborhood of the origin of the coordinate system, the second-order terms can be neglected. For the perspective projection of a planar surface undergoing a planar 3-D motion, therefore, the local velocity field can be approximated by a linear velocity field:

$$\dot{u} \approx (g_1 u + g_2 v)\left(\omega + \frac{V_x}{e}\right) + V_x$$

$$\dot{v} \approx 0. \tag{A8}$$

Appendix B

Maximum-Likelihood Recovery of σ and ω From *def*

Equation 7 shows that infinite pairs of σ and ω can produce the same *def*. Let us assume that σ and ω range from 0 to σ_{max} and ω_{max}, respectively. If we divide σ by σ_{max} (to create what we call "normalized σ," or $\overline{\sigma}$) and ω by ω_{max} (to create what we call "normalized ω," or $\overline{\omega}$) and *def* by the product $\sigma_{max}\,\omega_{max}$ (to create what we call "normalized *def*," or $\overline{def}$), then the equality expressed by Equation 7 holds: $\overline{def}$, $\overline{\sigma}$, and $\overline{\omega}$ are unitless and range from 0 to 1. Figure B1 (left panel) shows the loci of possible solutions for the normalized equation $\overline{def} = \overline{\sigma}\,\overline{\omega}$. Let us denote with s the curvilinear ordinate coinciding with the points of the hyperbola shown in Figure B1 (left panel), and let us choose a positive direction for s so that s increases as $\overline{\omega}$ increases. Let us also define the origin of s ($s = 0$), the point of the hyperbola that corresponds to $\overline{\sigma} = 1$. If we hypothesize that σ and ω (and, as a consequence, $\overline{\sigma}$ and $\overline{\omega}$) have uniform probability density functions, then it is possible to show that the probability function of s is

$$p(s(\overline{\omega}, \overline{\sigma})) = \frac{1}{\log\left(\frac{1}{def}\right)} \frac{1}{\sqrt{\overline{\omega}^2 + \overline{\sigma}^2}}, \tag{B1}$$

given $s = \int_0^s du$, where $du = \sqrt{d\overline{\omega}^2 + d\overline{\sigma}^2}$.

The most likely $\overline{\sigma}$, $\overline{\omega}$ pair, that is, the $\overline{\sigma}$, $\overline{\omega}$ pair that maximizes Equation B1, corresponds to the point closest to the origin of the hyperbola $\overline{def} = \overline{\sigma}\,\overline{\omega}$. This is the "normalized solution"

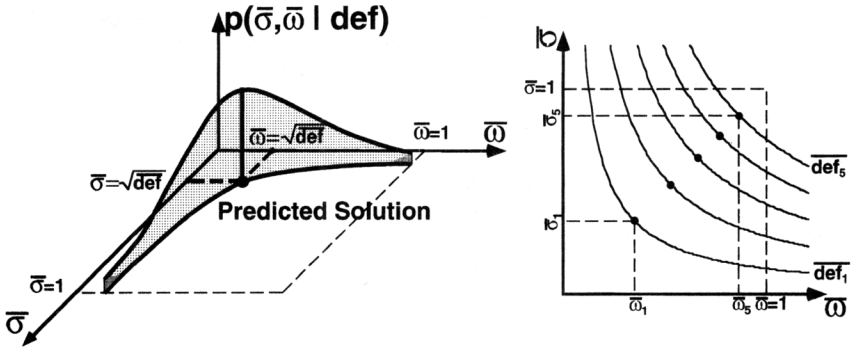

Figure B1. Left panel: Three-dimensional representation of the normalized $\bar{\sigma}, \bar{\omega}$ plane. The hyperbola drawn on the plane represents the loci of the $\bar{\sigma}, \bar{\omega}$ pairs compatible with a given $\overline{def}$ magnitude. The vertical dimension represents the probability density function $p(\bar{\sigma}, \bar{\omega}|\overline{def})$ for the considered $\overline{def}$ magnitude. The maximum of the probability density function corresponds to the $\bar{\sigma}, \bar{\omega}$ pair recovered from $\overline{def}$ by Equations 9 and 10. Right panel: The loci of the $\bar{\sigma}, \bar{\omega}$ pairs compatible with five $\overline{def}$ magnitudes in the $\bar{\sigma}, \bar{\omega}$ plane, together with the predictions of Equations 9 and 10.

$(\bar{\sigma} = \sqrt{\overline{def}}, \bar{\omega} = \sqrt{\overline{def}})$ and identifies the pair:

$$\omega = \sqrt{\frac{\omega_{max}}{\sigma_{max}}}\sqrt{def} = k\sqrt{def} \tag{B2}$$

$$\sigma = \sqrt{\frac{\sigma_{max}}{\omega_{max}}}\sqrt{def} = \frac{1}{k}\sqrt{def}. \tag{B3}$$

Proof: Let us indicate with σ and ω two random unitless variables with uniform probability densities in the range [0, 1]. Let us calculate the probability $p(\omega \leq \omega_0$ and $\sigma \leq \sigma_0)$, given that $\sigma\,\omega = def$:

$$p(\omega \leq \omega_0 \wedge \sigma \leq \sigma_0 | \omega\sigma = def). \tag{B4}$$

This probability can be calculated as

$$p(\omega \leq \omega_0 \wedge \sigma \leq \sigma_0 | \omega\sigma = def)$$

$$= \lim_{\epsilon \to 0} p(\omega \leq \omega_0 \wedge \sigma \leq \sigma_0 | def < \omega\sigma \leq def + \epsilon)$$

$$= \lim_{\epsilon \to 0} \frac{p(\omega \leq \omega_0 \wedge \sigma \leq \sigma_0 \wedge def < \omega\sigma \leq def + \epsilon)}{p(def < \omega\sigma \leq def + \epsilon)}. \tag{B5}$$

The meaning of Equation B5 can be better understood by considering Figure B2 (central panel). This figure shows two curves representing two hyperbolas defined by the equations $def = \sigma\omega$ and $(def + \epsilon) = \sigma\omega$. The probability that one σ, ω pair falls

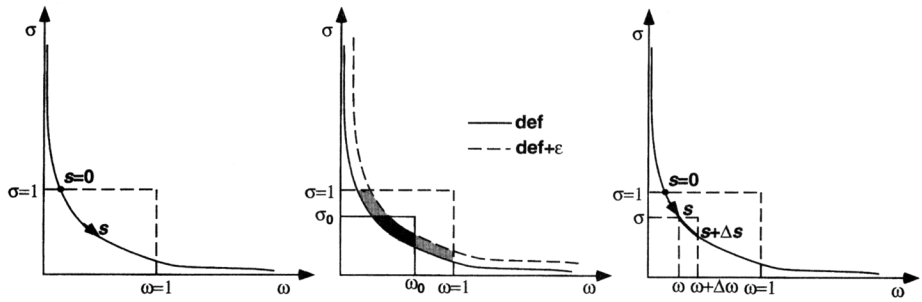

Figure B2. Left panel: The loci of the σ, ω pairs compatible with one def magnitude. The point $s = 0$ represents the origin of the curvilinear coordinate s. Central Panel: Two hyperbolas representing the loci of the σ, ω pairs compatible with two def magnitudes: def and $def + \epsilon$. The gray and black areas represent the loci of the σ, ω pairs compatible with deformations ranging between def and $def + \epsilon$ in the space delimited by σ_{max} ($\sigma = 1$) and ω_{max} ($\omega = 1$). The black area represents the loci of the σ, ω pairs compatible with deformations ranging between def and $def + \epsilon$ in the space delimited by σ_0, ω_0. Right Panel: The increment Δs of the curvilinear coordinate s and the associated increment $\Delta\omega$.

(Appendix continues)

within the black area of the figure, given the a priori knowledge that the pair falls within the gray area of the figure, is

$$p(\omega \leq \omega_0 \wedge \sigma \leq \sigma_0 | def < \omega\sigma \leq def + \epsilon).$$

Because we hypothesize uniform probability density functions for σ and ω, this probability is equal to the ratio between the black and gray areas. The limit of this ratio as ϵ tends to zero gives us the probability that the σ, ω pair falls within the portion of the hyperbola $def = \sigma\,\omega$ delimited by σ_0 and ω_0.

The numerator of Equation B5 is

$$p(\omega \leq \omega_0 \wedge \sigma \leq \sigma_0 \wedge def < \omega\sigma \leq def + \epsilon)$$

$$= \int_{def+\epsilon/\sigma_0} \left(\frac{\epsilon}{\omega}\right) d\omega + \left(\frac{\epsilon}{\sigma_0}\right)\sigma_0 - \int_{def/\sigma_0}^{def+\epsilon/\sigma_0} \left(\frac{def}{\omega}\right) d\omega$$

$$= \epsilon \log \frac{\omega_0\sigma_0}{def + \epsilon} + \epsilon - def\left(\log \frac{def + \epsilon}{def}\right) \quad \text{(B6)}$$

and the denominator of Equation B5 is

$$p(def < \omega\sigma \leq def + \epsilon) = \int_{def+\epsilon}^{1} \left(\frac{\epsilon}{\omega}\right) d\omega + \epsilon - \int_{def}^{def+\epsilon} \left(\frac{def}{\omega}\right) d\omega$$

$$= \epsilon \log \frac{1}{def + \epsilon} + \epsilon - def\left(\log \frac{def + \epsilon}{def}\right). \quad \text{(B7)}$$

The limit of the ratio between Equations B6 and B7 as ϵ tends to zero is

$$p(\omega \leq \omega_0 \wedge \sigma \leq \sigma_0 | \omega\sigma = def) = \frac{\log \dfrac{\omega_0\sigma_0}{def}}{\log \dfrac{1}{def}}. \quad \text{(B8)}$$

Now, let us consider one generic point ω, σ on the hyperbola $def = \sigma\omega$. This point individuates one curvilinear coordinate s (see Figure B1, right panel). The probability density of s is as follows:

$$p(s) = \lim_{\Delta s \to 0} \frac{P(s \leq s < s + \Delta s)}{\Delta s}$$

$$= \lim_{\Delta s \to 0} \frac{\dfrac{\log \dfrac{(\omega + \Delta\omega)\sigma}{def}}{\log \dfrac{1}{def}}}{\Delta s}$$

$$= \lim_{\Delta\omega \to 0} \frac{1}{\log \dfrac{1}{def}} \frac{\log \dfrac{(\omega + \Delta\omega)\dfrac{def}{\omega}}{def}}{\sqrt{1 + \dfrac{def^2}{\omega^4}}\,\Delta\omega}$$

$$= \frac{1}{\log \dfrac{1}{def}} \frac{1}{\sqrt{\omega^2 + \sigma^2}}$$

given that

$$\Delta s = \sqrt{1 + \frac{def^2}{\omega^4}}\,\Delta\omega.$$

Received November 25, 1996
Revision received February 5, 1998
Accepted March 16, 1998 ■